

1 **Climate variability in SE Europe since 1450 AD based on a varved sediment**
2 **record from Etoliko Lagoon (Western Greece)**

3

4 Andreas Koutsodendris^{1*}, Achim Brauer², Jane M. Reed³, Birgit Plessen², Oliver
5 Friedrich¹, Barbara Hennrich¹, Ierotheos Zacharias⁴, Jörg Pross¹

6

7 ¹ Institute of Earth Sciences, Heidelberg University, Im Neuenheimer Feld 234, 69120
8 Heidelberg, Germany

9 ² German Research Center for Geosciences, Section 5.2 Climate Dynamics and Landscape
10 Evolution, Telegrafenberg, 14473 Potsdam, Germany

11 ³ Geography, School of Environmental Sciences, University of Hull, Cottingham Road, Hull
12 HU6 7RX, UK

13 ⁴ Department of Environmental and Natural Resources Management, University of Patras,
14 Seferi 2, 30100 Agrinio, Greece

15

16 * Corresponding author (andreas.koutsodendris@geow.uni-heidelberg.de)

17

18 **Keywords:** Climate variability; Little Ice Age; Solar minimum; Varve microfacies; SE
19 Europe; Balkan Peninsula; Etoliko Lagoon

20

21 **Highlights:**

- 22 • Southernmost varve record from the Balkan Peninsula spanning the Little Ice Age
23 • Multiproxy sedimentological, paleoecological and geochemical analyses applied
24 • Enhanced productivity post-1740 AD due to increased nutrient input and
25 temperature
26 • Varve microfacies is highly sensitive to climate change from 1740 AD onwards

- 27 • Variability in precipitation assigned to North Atlantic Oscillation dynamics

28

29 **Abstract:**

30 To achieve deeper understanding of climate variability during the last millennium in
31 SE Europe, we report new sedimentological and paleoecological data from Etoliko
32 Lagoon, Western Greece. The record represents the southernmost annually
33 laminated (i.e., varved) archive from the Balkan Peninsula spanning the Little Ice
34 Age, allowing insights into critical time intervals of climate instability such as during
35 the Maunder and Dalton solar minima. After developing a continuous, ca. 500-year-
36 long varve chronology, high-resolution μ -XRF counts, stable-isotope data measured
37 on ostracod shells, palynological (including pollen and dinoflagellate cysts), and
38 diatom data are used to decipher the season-specific climate and ecosystem
39 evolution at Etoliko Lagoon since 1450 AD. Our results show that the Etoliko varve
40 record became more sensitive to climate change from 1740 AD onwards. We
41 attribute this shift to the enhancement of primary productivity within the lagoon, which
42 is documented by an up to threefold increase in varve thickness. This marked
43 change in the lagoon's ecosystem was caused by: (i) increased terrestrial input of
44 nutrients, (ii) a closer connection to the sea and human eutrophication particularly
45 from 1850 AD onwards, and (iii) increasing summer temperatures. Integration of our
46 data with those of previously published paleolake sediment records, tree-ring-based
47 precipitation reconstructions, simulations of atmospheric circulation and instrumental
48 precipitation data suggests that wet conditions in winter prevailed during 1740–1790
49 AD, whereas dry winters marked the periods 1790–1830 AD (Dalton Minimum) and
50 1830–1930 AD, the latter being sporadically interrupted by wet winters. This
51 variability in precipitation can be explained by shifts in the large-scale atmospheric
52 circulation patterns over the European continent that affected the Balkan Peninsula
53 (e.g., North Atlantic Oscillation). The transition between dry and wet phases at

54 Etoliko points to longitudinal shifts of the precipitation pattern in the Balkan Peninsula
55 during the Little Ice Age.

56

57 **1. Introduction**

58 Representing one of the strongest global climate instabilities during the Holocene,
59 the Little Ice Age (LIA) is marked by a multi-centennial-long cooling (14th – 19th
60 centuries AD) that preceded the recent ‘global warming’ of the 20th century (e.g.,
61 Mayewski et al., 2004; Mann et al., 2009; Büntgen et al., 2011; PAGES 2k
62 Consortium, 2013). The cooling has been predominantly attributed to reduced solar
63 activity and was particularly pronounced during the 1645–1715 AD and 1790–1830
64 AD solar minima, which are known as Maunder and Dalton Minima, respectively
65 (e.g., Mann et al., 1998, 2009; Jones and Mann, 2004). Although cooler conditions
66 prevailed generally in both hemispheres between 1580 and 1880 AD, the climate
67 during the LIA is characterized by remarkable spatiotemporal heterogeneity (Mann et
68 al., 2009; Ljungqvist et al., 2012; PAGES 2k Consortium, 2013). This heterogeneity is
69 particularly well documented for the European continent (Luterbacher et al., 2004;
70 Matthews and Briffa, 2005; Xoplaki et al., 2005), where changes in atmospheric
71 circulation are known to have affected temperature and precipitation regionally (e.g.,
72 Luterbacher et al., 2010, 2012; Ljungqvist et al., 2016). This holds particularly true for
73 the circum–Mediterranean region (Touchan et al., 2005; Griggs et al., 2007; Nicault
74 et al., 2008; Gogou et al., 2016). For that region, a compilation of lake, tree-ring and
75 marine climate records has provided evidence for more humid conditions on the
76 Iberian Peninsula and in NW Africa during the LIA, in contrast to Asia Minor and the
77 Levant that were characterised by drier conditions (Roberts et al., 2012).

78 The Balkan Peninsula is located between the higher-latitude (i.e., Westerlies and
79 East Russian/Siberian High) and lower-latitude (i.e., African Monsoon) climate
80 systems (Lionello et al., 2012). Despite this strategic position that can yield insight

81 into the interplay of both climate systems through time, climate variability during the
82 LIA on the Balkan Peninsula has remained largely unexplored. Available tree-ring
83 reconstructions (Trouet, 2014; Klesse et al., 2015; Levanic et al., 2015) and evidence
84 for expansion of glaciers in Montenegro (Hughes, 2009) suggest cooling during the
85 LIA across the Balkans. However, there is contrasting evidence between the Western
86 and the Eastern Balkan Peninsula, generating debate as to whether this cooling was
87 associated with wetter or drier conditions. More specifically, $\delta^{18}\text{O}_{\text{calcite}}$ records from
88 Lake Ohrid and Lake Prespa (Figure 1; Leng et al., 2013; Lacey et al., 2014) suggest
89 that the Western Balkan Peninsula experienced wet conditions during the last
90 millennium, which allowed the expansion of glaciers in Montenegro (Hughes, 2009).
91 In contrast, tree-ring reconstructions from Mt. Olympus (SE Balkans; Figure 1)
92 suggest drier conditions during the LIA than the 1950–2010 average (Klesse et al.,
93 2015), which is in agreement with paleoclimatic data from Lake Dojran (Figure 1) that
94 also document dry conditions in the SE Balkans during the last millennium (Zhang et
95 al., 2014).

96 The seasonal precipitation variability during the LIA is also insufficiently constrained
97 on the Balkans (e.g., between the Eastern and Western Peninsula). Tree-ring-based
98 model results have suggested that the Balkan Peninsula experienced alterations
99 between dry (e.g., 1540–1575, 1620–1640, 1760–1780 AD) and wet (e.g., 1700–
100 1750 AD) spring/summer periods (Nicault et al., 2008), which were punctuated by a
101 series of extreme wet or dry spring/summers (e.g., Griggs et al., 2007). Furthermore,
102 sedimentological and geochemical data from Lake Butrint in the Western Balkans
103 (Figure 1) suggest that although the LIA was generally characterized by higher
104 humidity relative to pre- and post-LIA times, maximum winter precipitation prevailed
105 between 1600 and 1800 AD (Morellón et al., 2016). Moreover, historical information
106 has documented several extreme wintertime floods and droughts locally across the
107 Balkans (Xoplaki et al., 2001; Luterbacher et al., 2010). Current understanding of

108 seasonal hydrological variability during the LIA is clearly hampered by the scarcity of
109 high-resolution climate records and the existence of contradictory data, but also by
110 uncertainties in disentangling the effects of climate forcing *versus* human impact on
111 climate proxy records considering the substantial socio-economic changes in the
112 region during the last millennium (e.g., Gogou et al., 2016; Morellón et al., 2016;
113 Xoplaki et al., 2016).

114 Annually laminated (i.e., varved) sediment records have been successfully employed
115 to decipher LIA climate dynamics from different parts of Europe (e.g., Czymzik et al.,
116 2010; Corella et al., 2012, 2014; Swierczynski et al., 2012) because they allow
117 multiproxy high-resolution analyses on seasonal timescales (e.g., Brauer, 2004;
118 Ojala et al., 2012; Zolitschka et al., 2014). To date, however, varve-based studies
119 from the Balkan Peninsula are still rare (Ariztegui et al., 2010; Koutsodendris et al.,
120 2015), and only one of the current records spans the LIA (Morellón et al., 2016). As
121 such, the potential of varved archives in reconstruction of climate change in SE
122 Europe during the last millennium has remained largely unexplored. To contribute to
123 a better understanding of the interactions between climate variability and human
124 influence during the LIA on the Balkan Peninsula, we present a new, continuously
125 varved sediment record from Etoliko Lagoon (Western Greece; Figure 1) extending
126 back to 1450 AD. We apply a multiproxy approach including sedimentological (varve
127 counting and microfacies), geochemical (μ -XRF scanning, $\delta^{13}\text{C}_{\text{ostracods}}$ and
128 $\delta^{18}\text{O}_{\text{ostracods}}$) and paleoecological (pollen, dinoflagellate cysts and diatoms) analyses,
129 and pair our results with available instrumental and proxy data from continental
130 Europe and the greater Mediterranean region.

131

132 **2. Regional setting**

133 Etoliko Lagoon is a deep (~30 m maximum depth), anoxic lagoon that is part of an
134 extensive complex of wetlands along the Ionian coast of Western Greece (Figure 1).

135 It is connected via a small, <200-m-long opening to the shallow (<2 m deep)
136 Messolonghi Lagoon, which itself is connected to the Ionian Sea ~12 km south of
137 Etoliko (Figure 2). Because of this particular lagoonal morphology, enhanced
138 seawater intrusion occurs when southern winds prevail, as has been documented by
139 instrumental data for the past ~10 years (Gianni et al., 2011). The catchment area of
140 Etoliko Lagoon currently comprises ~71 km²; it is naturally drained by few, ephemeral
141 streams. Since the 1940's, the hydrology of the catchment area has been strongly
142 affected by the installation of irrigation channels and pumping stations (Gianni et al.,
143 2011). In-depth information on the morphology of the lagoon and the regional setting
144 has been provided by Vött et al. (2006) and Koutsodendris et al. (2015).

145 Given its location on the SW Balkan Peninsula (Figure 1), Etoliko Lagoon and its
146 surroundings are characterized by typical Mediterranean climate conditions, with dry
147 summers and wet winters (Lionello et al., 2012). Based on available meteorological
148 data from the towns of Etoliko and Agrinio (~20 km north of Etoliko Lagoon; Figure
149 2), the mean annual temperature since 1952 is 17.3 °C (mean winter: 9.0 °C; mean
150 summer: 26.4 °C), and mean annual precipitation since 1947 is 915 mm (Hellenic
151 National Meteorological Service, unpublished). The seasonal distribution of
152 precipitation is strongly skewed towards the fall, winter and spring seasons, with ~41
153 % of precipitation occurring in December–February, ~21 % in March–May, ~7 % in
154 June–August, and ~33 % in September–November.

155

156 **3. Material and Methods**

157 Sediment cores from Etoliko Lagoon were retrieved in October 2012 using a
158 UWITEC coring device from a small catamaran platform designed at GFZ Potsdam.
159 Two 2-m-long cores (ETO12-2 and ETO12-3) were recovered from 28 m water depth
160 in the northern part of the lagoon (38° 28' 52" N / 21° 18' 56" E; Figure 2).
161 Correlation of the cores was achieved using magnetic susceptibility downcore

162 profiles that were generated using a Bartington MS2E sensor (Nowaczyk, 2001), as
163 well as microfacies analysis (Figure 3).

164 Thin sections (size: 120x35 mm) for varve counting were prepared following
165 standard techniques comprising freeze-drying, impregnation with Araldite 2020
166 epoxy resin under vacuum, sawing, and grinding (Brauer and Casanova, 2001).
167 Successive thin sections with an overlap of 2 cm were analysed to warrant continuity
168 of observations. Varve microfacies analysis was carried out with a petrographic
169 microscope at 100–400x magnification, allowing the precise description and
170 measurement of the seasonal sub-layer thicknesses (Brauer et al., 2008;
171 Koutsodendris et al., 2011).

172 Element geochemical measurements were carried out on the epoxy-resin-
173 impregnated sediment blocks using a micro-X-ray fluorescence (μ -XRF) EAGLE III
174 XL spectrometer (200 μ m step size, 10 s count time, 30 kV tube voltage, and 30 mA
175 tube current) (Dulski et al., 2015). In addition, 50 ostracod samples were analyzed for
176 $\delta^{18}\text{O}$ and $\delta^{13}\text{C}$ at GFZ Potsdam using a KIEL IV carbonate device coupled to a
177 MAT253 Thermo Fisher isotope ratio mass spectrometer. Sufficient amounts of
178 ostracod shells for isotope analyses were generally found every 1–2 cm throughout
179 the study interval, yielding a mean temporal resolution of ~9 years (range: 2–31
180 years). About 50 μ g were automatically treated with 103 % H_3PO_4 at 72 °C, and the
181 isotopic composition was measured on the released and cryogenic purified CO_2 . All
182 results are reported in δ notation relative to V-PDB. Replicate analysis of reference
183 material (NBS19) yielded standard errors of 0.04 ‰ for $\delta^{13}\text{C}$ and 0.06 ‰ for $\delta^{18}\text{O}$,
184 respectively.

185 In total, 32 diatom and 34 pollen samples, each comprising ~4 cm^3 of sediment, were
186 analyzed for the core interval between 1450 and 1930 AD, yielding a mean temporal
187 resolution of ~15 years (range: 6–30 years). The palynological preparation followed
188 standard techniques, including sediment freeze-drying, weighing, treatment with HCl

189 (>30 %) and HF (40 %), sieving (10 µm), and mounting on glass slides with Dymax
190 425TM. Pollen samples were spiked with known quantities of *Lycopodium* spores
191 (Lund University, Batch No. 482316) to allow calculation of absolute concentrations.
192 Diatom preparation followed standard techniques including heating with 25–30 ml
193 H₂O₂ (30 %), a few drops of HCl (>30 %), cleaning by centrifuging with deionised
194 water, and mounting on glass slides using NaphraxTM (Battarbee et al., 2001). An
195 average of 323 pollen grains (excluding pollen from aquatics and spores) and 422
196 diatom valves were counted per sample; minimum sums for both pollen and diatom
197 analysis were always above 300 grains and valves, respectively, per sample. Finally,
198 dinoflagellate cysts (dinocysts) were also counted when present in the palynological
199 samples, resulting in an average of 66 dinocysts (range: 15–338 specimens) per
200 sample.

201

202 **3.1 Varve chronology**

203 The correlation of the two cores from Etoliko Lagoon allowed the establishment of a
204 100-cm-long composite record of laminated sediments. These laminated sediments
205 are built up by two distinct, alternating sub-layers: a light one consisting mainly of
206 calcite and a dark one consisting of organic-rich material. They represent
207 sedimentation during spring/summer and autumn/winter, respectively (see
208 Koutsodendris et al., 2015, for a detailed description). The interpretation that the
209 laminated sediments at Etoliko Lagoon represent true varves has been further
210 confirmed by ¹³⁷Cs dating (Koutsodendris et al., 2015). For the composite sediment
211 profile available from Etoliko (spanning from 1450 to 2011), a total of 514 varves
212 were counted. For short intervals within the lowermost 20 cm of the composite record
213 where varve preservation is poor or the sediment was disturbed during coring, age
214 interpolations were performed based on the average thickness of 10 varves
215 deposited directly below and above the respective interval. In this study, we focus on

216 the interval prior to 1930 AD because the environmental signals recorded in the
217 sediments of Etoliko Lagoon over the last seven decades have been predominantly
218 caused by anthropogenic influence (Koutsodendris et al., 2015).

219

220 **4. Results**

221 **4.1 Sedimentology, elemental and stable-isotope geochemistry**

222 Throughout the studied interval, the total varve thickness is 1.35 mm on average
223 (SD: 0.76; range: 0.25–4.59 mm); varve thickness increases after 1740 AD from a
224 mean of 0.87 mm (SD: 0.41; range: 0.25–2.32 mm) to a mean of 1.93 mm (SD: 0.69;
225 range: 0.43–4.59 mm) (Figure 4). The thickness of the calcite sub-layers is 0.35 mm
226 on average, varying between 0.0 and 1.26 mm (SD: 0.26); their thickness increases
227 from a mean of 0.22 mm (SD: 0.12; range: 0.05–1.26 mm) prior to 1740 AD to a
228 mean of 0.51 mm (SD: 0.30; range: 0.03–1.49 mm) thereafter. Distinct calcite sub-
229 layers are not registered for the 1882–1891 AD period; the spring/summers sub-
230 layers during that time are dominated by the large (often >100 μm) centric diatom,
231 *Actinocyclus* cf. *octonarius*. Aragonite replaces calcite in spring/summer sub-layers of
232 two years, i.e., 1884 and 1920 AD. The thickness of the organic-rich sub-layers is
233 0.96 mm on average (SD: 0.61; range: 0.13–3.79 mm). Similar to the calcite sub-
234 layers, the thickness of organic-rich sub-layers increases after 1740 AD from 0.65
235 mm on average (SD: 0.36; range: 0.13–2.12 mm) to 1.35 mm (SD: 0.64; range:
236 0.13–3.79 mm). Deposition of large centric diatoms occurred below (and rarely
237 within) the calcite sub-layers. These diatoms often form distinct sub-layers from 1780
238 onwards, with the thickest sub-layers having been deposited during the 1882–1895
239 AD period. In addition, skeletons of the silicoflagellate *Dictyocha fibula* were
240 deposited after calcite deposition from 1866 AD onwards, forming distinct sub-layers
241 during the 1890–1915 AD period; silicoflagellate sub-layers are also present from
242 1652 until 1665 AD (Figure 4).

243 The μ -XRF core-scanning results document a shift in the interannual variability of Ca
244 and Ti counts around 1760 AD (Figure 5). Calcium shows a coherent pattern with the
245 calcite sub-layer thickness data (compare Figure 4), with increasing Ca counts
246 registered during 1740–1880 AD and decreasing during 1880–1920 AD; this
247 suggests that Ca mainly reflects the endogenic calcite content in the biogenic varves
248 (e.g., Corella et al., 2014). The total counts of Ti, which is an indicator for increased
249 clastic input (e.g., Martin-Puertas et al., 2011; Corella et al., 2012; Neugebauer et al.,
250 2015; Morellón et al., 2016), are increased between 1680 and 1910 AD with an
251 exception during 1810–1840 AD that is marked by lower counts (Figure 5). In
252 agreement, the Ti/Ca ratios are high during 1740–1910 AD, and low during 1790–
253 1840 AD (Figure 5). The Fe/Mn ratios, which increase under enhanced anoxic
254 conditions (e.g., Martin-Puertas et al., 2011; Corella et al., 2012; Morellón et al.,
255 2016), are high during 1740–1790 and 1840–1910 AD and low during 1790–1840
256 AD; transiently, low values also prevail around 1890 AD (Figure 5). The Si/Ti ratios,
257 which are used as an indicator for diatom productivity (e.g., Kienel et al., 2013;
258 Morellón et al., 2016), are high during 1680–1840 AD and low during 1640–1680 and
259 1840–1910 AD (Figure 5). Finally, the Sr/Ca ratios, which increase with increasing
260 salinity (e.g., Martin-Puertas et al., 2011), show high values during 1640–1680 and
261 1840–1930 AD, and low values during 1680–1840 AD (Figure 5).

262 Carbon isotope values measured on ostracod shells ($\delta^{13}\text{C}_{\text{ostracod}}$) as a measure of
263 organic matter input into the lagoon (e.g., Schwalb, 2003) vary between -9.9 and -6.5
264 ‰. Low values occur during the 1690–1730 and 1765–1800 AD periods, with
265 transient minima also occurring between 1855 and 1895 AD. In contrast, high values
266 persist during the 1810–1840 AD period (Figure 4). The oxygen isotope values
267 measured on ostracod shells ($\delta^{18}\text{O}_{\text{ostracod}}$) as an indicator of salinity changes (e.g.,
268 Schwalb, 2003) vary between -2.6 and 0.4 ‰. They exhibit considerable variability,
269 with particularly high amplitudes of fluctuation from 1850 AD onwards (Figure 4).

270

271 **4.2 Biotic signals**

272 The interval between 1450 and 1850 AD is characterized by no remarkable changes
273 in the pollen percentages of the individual groups of taxa, whereas an increase in the
274 percentages of cultivated plants at the expense of Mediterranean sclerophylls and
275 deciduous trees occurs from 1850 AD onwards (Figure 6). Throughout the studied
276 interval, Mediterranean sclerophylls (including *Cistus*, *Ephedra*, Ericaceae, *Hedera*,
277 *Juniperus*, *Laurus nobilis*, *Myrtus*, *Phillyrea*, *Pistacia*, and *Quercus* evergreen) form
278 the most dominant pollen group, accounting for 24.6 % on average in each sample
279 (range: 16.9–36.6 %). Pollen grains from cultivated plants (including Cerealia, *Olea*
280 and *Vitis*) comprise 20.5 % on average (range: 11.4–30.6 %), followed by
281 riparian/salt marsh herbs (including Chenopodiaceae, Poaceae, Plantaginaceae,
282 Ranunculaceae, *Rumex*, and *Thalictrum*) and deciduous trees (including *Corylus*,
283 *Carpinus/Ostrya*, *Juglans*, *Quercus* deciduous, and *Ulmus*) that account for 20.3 %
284 (range: 0.0–26.4 %) and 17.2 % (11.5–25.6 %), respectively. Riparian trees/shrubs
285 (including *Alnus*, *Fraxinus*, *Platanus*, *Rubus saxatilis*, *Salix*, *Tamarix*, and *Vitex*) and
286 other herbs comprise 5.9 % (range: 3.0–9.0 %) and 5.5 % (0.0–8.9 %), respectively.
287 Finally, pollen from conifers (including *Abies* and *Pinus*) accounts for 3.4 % (range:
288 0.9–7.2 %).

289 Among the dinocysts in the Etoliko sediments since 1450 AD, cysts of phototrophic
290 representatives (including *Lingulodinium machaerophorum* and *Spiniferites* sp.) are
291 dominant; they account for 61.3 % on average (range: 12.4–97.9 %) (Figure 6).
292 Heterotrophic dinocysts (including *Brigantedinium* sp., *Dubridinium* sp., *Echinidinium*
293 sp., *Gymnodinium noleri/microreticulatum*, *Polykrikos schwarzii*, and *Votadinium*
294 *calvum*) account for 38.4 % (range: 2.1–86.7 %). Both photo- and heterotrophic
295 dinoflagellates registered at Etoliko sediments typically thrive in coastal and brackish
296 environments of the Ionian and Aegean seas in the Eastern Mediterranean (e.g.,

297 Kotthoff et al., 2011; Triantaphyllou et al., 2014; Balkis et al., 2016). An increase in
298 the percentages of heterotrophic dinocysts at the expense of phototrophic cysts is
299 documented between 1850 and 1920 AD (Figure 6).

300 In total, 55 diatom taxa were recorded in the studied material. Planktonic taxa
301 dominate the diatom assemblages and account for 76.2 % of total diatoms on
302 average (range: 39.1–96.9 %); benthic taxa comprise 23.8 % on average (range:
303 3.1–60.9 %) (Figure 7). A distinct increase in the percentage of benthic taxa at the
304 expense of planktonic taxa (~30 %) occurs from 1790 to 1820 AD. The dominant
305 planktonic taxa comprise small (<25 µm in diameter) centric *Cyclotella*
306 *choctawhatcheeana* and *Cyclotella atomus*, which together account for 71.5 % on
307 average. Other common planktonic taxa comprise *Actinocyclus octonarius*, *Cyclotella*
308 *ocellata*, *C. meneghiniana*, *Chaetoceros* spp., and *Melosira sol.* Most common
309 benthic taxa belong to the genera *Amphora*, *Cocconeis*, *Diploneis*, *Mastogloia*,
310 *Navicula*, *Nitzschia*, *Opephora*, and *Synedra*. In general, both planktonic and benthic
311 diatom assemblages of the studied Etoliko sediments are dominated by
312 marine/brackish species, which are typical in coastal and brackish environments
313 (e.g., Gilabert, 2001; Reed et al., 2001; Miho and Witkowski, 2005; Weckström and
314 Juggins, 2005), with sporadic occurrence of freshwater taxa (e.g., *Stephanodiscus*
315 sp.) (e.g., Reed et al., 2012). The diatom assemblages are dominated by
316 *Thalassionema nitzschioides*, *Chaetoceros* spp. and *Pseudonitzschia calliantha* from
317 ~1970 onwards (Figure 7), when Etoliko Lagoon experienced severe human-induced
318 eutrophication (Koutsodendris et al., 2015). Notably, the diatom flora of Etoliko
319 includes marine benthic taxa that are not known from inland salt lake salinity training
320 sets (Juggins 2001), including *Ardissonea* sp., *Cocconeis scutellum*, *Dimeregramma*
321 *minor*, and *Gomphonemopsis obscurum* (Witkowski et al., 2000; Resende et al.,
322 2007). Finally, increased occurrence of siliceous remains of the coastal brown alga,

323 *Dictyocha fibula*, is recorded sporadically during the 1590–1630 and 1680–1730 AD
324 periods, with regular presence from 1860 AD to the present.

325

326 **5. Discussion**

327 The Etoliko varve record represents the first annually resolved archive from the
328 southern Balkan Peninsula spanning the past 500 years. Considering the general
329 lack of varved records from SE Europe spanning the last millennium (e.g., Ojala et
330 al., 2012; Zolitschka et al., 2014; Morellón et al., 2016), the new record from Etoliko
331 can provide valuable insights into the climate variability of this region during the past
332 five centuries, and notably across the LIA. The most striking feature of the Etoliko
333 varve record is a two- to three-fold increase in varve thickness after 1740 AD, which
334 is apparent in both the organic-rich (autumn/winter) and calcite (spring/summer) sub-
335 layers (Figure 4). In the following, we discuss the evolution of Etoliko Lagoon for the
336 periods before and after this transition, i.e., 1450–1740 AD and 1740–1930 AD,
337 focusing on the paleoenvironmental and paleoclimatic factors that may have
338 impacted the aquatic ecosystem, including nutrient input, temperature, and
339 anthropogenic impact.

340

341 **5.1 1450–1740 AD**

342 The interval between 1450 and 1740 AD at Etoliko is characterized by the deposition
343 of considerably thinner varves than from 1740 AD onwards, with varve thickness
344 rarely exceeding 1.5–2.0 mm (Figure 4). The fact that the organic-rich and calcite
345 varve sub-layer thickness shows little variability suggests the prevalence of stable
346 conditions in the aquatic ecosystem during this interval and/or the low fidelity of the
347 varves from that time in recording environmental and climate change. To resolve this
348 question, we focus on the Maunder solar minimum period (1645–1715 AD). Because

349 the Maunder Minimum represents the climax of the LIA in Europe (e.g., Luterbacher
350 et al., 2004; PAGES 2k Consortium, 2013) and had a strong climatic impact on the
351 Balkan Peninsula (Xoplaki et al., 2001), it is reasonable to assume that the Maunder
352 Minimum substantially impacted the aquatic system of Etoliko Lagoon.

353 In contrast to the low variability in the sub-layer thickness during the Maunder
354 Minimum, other proxy data do point to considerable environmental change at Etoliko
355 during that time (Figure 4). Specifically, the onset of the Maunder solar minimum is
356 marked by the formation of distinct silicoflagellate sub-layers (Figure 4), an increase
357 of the heterotrophic dinocysts (Figure 6), and an increase in the abundance of the
358 planktonic diatom *Cyclotella atomus* (Figure 7). While the ecological tolerance ranges
359 of the dominant planktonic diatoms are too wide to be definitive (e.g., Weckström and
360 Juggins, 2005; Reed et al., 2012), these observations suggest changes in salinity
361 and nutrient availability in the aquatic environment may have occurred at Etoliko.
362 During the younger part of the Maunder Minimum, the μ -XRF data show an
363 increasing trend in Ti concentrations (Figure 5) representing an increase in clastic
364 input. Accordingly, an increase in fresh-water input would reduce the salinity of the
365 lagoon, a view that is supported by the coeval decrease of the Sr/Ca ratios (Figure
366 5). A scenario of enhanced terrestrial input over the course of the Maunder Minimum
367 is also supported by a trend to lighter $\delta^{13}\text{C}_{\text{ostracod}}$ values between 1660 and 1710 AD
368 (Figure 4) suggesting a higher input of terrestrial organic matter (e.g., Schwalb,
369 2003). This would increase nutrient availability in the water column promoting diatom
370 blooms, which is in agreement with the increase of the Si/Ti ratios after 1680 AD
371 (Figure 5). Notably, palynological data indicate that the vegetation in the catchment
372 of the lagoon remained stable during the Maunder Minimum, with only very minor
373 changes in the percentages of all terrestrial plant groups (Figure 6). While increased
374 transport of clastic and organic matter into the lagoon might result from enhanced
375 erosion due to reduced vegetation cover, the catchment stability suggests an

376 alternate explanation, namely that the increased terrestrial input into the lagoon was
377 caused by an increase in precipitation. These findings are in accordance with tree-
378 ring reconstructions from the Mediterranean region (Nicault et al., 2008) as well as
379 historical data from the southern Balkan Peninsula that both document relatively wet
380 conditions during 1675–1715 AD (Xoplaki et al., 2001). In conjunction, these lines of
381 evidence document that the environment around Etoliko Lagoon was affected by
382 climate change during the Maunder Minimum. In addition, the implication is that the
383 varve thickness data from Etoliko are not particularly sensitive to climate change
384 during the 1450–1740 AD period.

385

386 **5.2 1740–1930 AD**

387 The varve thickness at Etoliko from 1740 until 1930 AD is 2–3 times higher than
388 during 1450–1740 AD, and exhibits a stronger variability (Figure 4). Following the
389 rationale discussed in the section above, the question emerges as to whether the
390 Etoliko varve archive became more sensitive to climate forcing from 1740 AD
391 onwards and, if so, which factors were responsible for this change in the aquatic
392 environment of the lagoon. The possibility that other scenarios exist that may explain
393 the observations made also needs to be explored. To address this issue, and
394 considering that solar forcing was an important driver for climate change during the
395 LIA (e.g., Mann et al., 1998, 2009; Jones and Mann, 2004; PAGES 2k Consortium,
396 2013), we have compared the Etoliko varve thickness data with total solar irradiance
397 trends generated by ¹⁰Be measurements on Antarctic ice cores (Delaygue and Bard,
398 2011). Strikingly, the variability in thickness of the Etoliko varves closely mimics total
399 solar irradiance from 1740 AD onwards (Figure 8). Specifically, the thickness data
400 show maximum values synchronously with the solar peaks at ~1740 and ~1785 AD,
401 a subsequent decrease during the 1790–1830 AD period (i.e., the Dalton Minimum;
402 see also Section 5.2.2 below), and similar trends during the 19th and 20th centuries

403 (Figure 8). It has been shown previously that changes in solar activity can affect
404 varve deposition in Europe (Martin-Puertas et al., 2012; Czymzik et al., 2013),
405 because solar activity influences the dynamics of the atmosphere (Gray et al., 2010;
406 Woollings et al., 2010) and ultimately influences sedimentation processes in lakes by
407 changing wind regimes and related wave activity. The close correspondence
408 between varve thickness at Etoliko and solar irradiance trends supports the view that
409 the Etoliko ecosystem became very sensitive to climate change from 1740 AD
410 onwards. Considering that the thickness of both the organic-rich and the calcite sub-
411 layers increases after 1740 AD, the increased climate sensitivity of the Etoliko varve
412 archive may have been triggered by a strengthening of the lagoon's productivity
413 throughout the year. In the following, we examine the individual proxy data from
414 Etoliko to understand more deeply the processes involved.

415 Enhanced nutrient input into Etoliko Lagoon could have resulted from three potential
416 sources: terrestrial runoff, inflow of marine waters and human-induced
417 eutrophication. A strong increase in the XRF-based Ti/Ca ratios provides strong
418 evidence for increasing terrestrial runoff from 1740 AD onwards (Figure 8). This
419 scenario is supported by the increased presence of the green alga *Pseudoschizaea*
420 sp. after 1740 AD (Figure 8), which is an indicator of freshwater input into brackish
421 environments (e.g., Mudie et al., 2010, 2011). Both observations suggest that Etoliko
422 Lagoon received enhanced terrestrial input after 1740 AD, increasing the nutrient
423 availability in the water column. This would ultimately lead to higher primary
424 productivity in the lagoon, an assumption which is in agreement to the peaking of the
425 Si/Ti ratios around 1750–1780 AD (Figure 6). In addition, the formation of distinct
426 silicoflagellate varve sub-layers (Figure 4) and the increase in the concentration of
427 marine dinoflagellate cysts (Figure 8) after 1850 AD suggest a stronger connection of
428 Etoliko Lagoon to the marine realm. As such, the marine realm could have also been
429 a source of nutrients particularly after 1850 AD. To assess the potential role of

430 human-induced eutrophication of the lagoon, we have employed the palynological
431 results to evaluate land use changes, as historical data of human activities in the
432 catchment area are absent. Although no remarkable changes in vegetation dynamics
433 occurred over the past 500 years, an increase in the percentage of cultivated plants
434 at the expense of Mediterranean sclerophylls and deciduous trees is apparent from
435 1850 AD onwards (Figure 6). This suggests clearance of the natural vegetation
436 around Etoliko Lagoon for agricultural purposes, which may have favored soil erosion
437 and further input of terrestrial nutrients in the lagoon. This scenario is in concert with
438 peaking Ti/Ca values post-1850 AD (Figure 4). In summary, our data suggest that
439 nutrient availability at Etoliko Lagoon increased in two steps: (i) after 1740 AD due to
440 higher terrestrial input associated with increased precipitation in the catchment of the
441 lagoon, and (ii) after 1850 AD due to stronger marine influence and higher terrestrial
442 input associated with land-use changes in the catchment. By extension, this resulted
443 in increased deposition of organic matter and formation of thicker organic-rich sub-
444 layers than prior to 1740 AD (Figure 8).

445 In contrast to the organic-rich sub-layers, the variability in thickness of the calcite
446 sub-layers does not mimic the total irradiance trend despite a two- to threefold
447 increase in absolute thickness (Figure 8). This suggests that the spring/summer
448 season, when biologically (algal) induced calcite precipitation forms the calcite sub-
449 layers (Koutsodendris et al., 2015), may have not been affected by the variability of
450 total annual irradiance. Interestingly, the thickness variability of the calcite sub-layers
451 closely resembles the mean European atmospheric temperature reconstructions for
452 summer (June-July-August) (Luterbacher et al., 2004; Xoplaki et al., 2005). Notably,
453 they show a similar increase during the 1740–1880 AD and a decrease during the
454 1880–1920 AD periods. The correspondence of the calcite sub-layer thickness with
455 summer air temperature is also supported by available regional instrumental data
456 from Athens (Arseni-Papadimitriou and Maheras, 1991) and Kerkyra (Mariolopoulos

457 et al., 1985) (see Figure 1 for locations). These observations reveal a link between
458 the productivity of Etoliko Lagoon and the shift to higher summer temperatures at
459 ~1740 AD. We, therefore, suggest that the strengthening of calcite deposition was
460 the result of enhanced algal blooms due to increased summer temperatures after
461 1740. Stronger algal blooms would reduce the CO₂ concentration in the water
462 column via respiration and, thereby, decrease of the CO₂/H₂CO₃⁻ ratio, ultimately
463 enhancing Ca precipitation and deposition of thicker calcite sub-layers (e.g., Brauer,
464 2004). A close look at the diatom data reveals a shift to greater dominance of the
465 smaller centric, *Cyclotella atomus*, over *C. choctawhatcheeana* (Figure 7) suggesting
466 a change in ecosystem dynamics. Both *Cyclotella atomus* and *C.*
467 *choctawhatcheeana*, and the morphologically similar taxon, *C. caspia* (often
468 confused with *C. choctawhatcheeana*; Genkal 2012), are common components of
469 phytoplankton succession in eutrophic Mediterranean lagoons (Sarno et al., 1993;
470 Miho and Witkowski, 2005). As noted, these taxa have wide ecological tolerance
471 ranges. Rather than being indicative of changes in productivity, the shift to
472 dominance of smaller *Cyclotella* species could instead be a response to warming
473 related to enhanced water column stratification and decreasing sinking velocity of
474 diatoms (Winder et al., 2009). At Etoliko, supporting evidence for enhanced water
475 column stratification comes from increasing Fe/Mn values after 1740 AD (Figure 5).
476 Based on this line of evidence, the diatom flora supports the scenario of temperature
477 control on increased calcite precipitation at Etoliko after 1740 AD.

478 To conclude, the Etoliko varves exhibit a strong response to climate change from
479 1740 AD onwards. We attribute this sudden shift towards higher sensitivity to an
480 increase in primary productivity of the lagoon beyond a critical threshold that was
481 caused by enhanced input of organic matter and increasing air temperatures.

482

483 **5.3 Precipitation variability from the mid-18th to mid-20th centuries**

484 The high fidelity of the Etoliko varves in recording climate change from 1740 AD
485 onwards provide insights into precipitation variability on the Western Balkan
486 Peninsula over the past two centuries. On the basis of instrumental measurements,
487 maximum precipitation at Etoliko occurs during winter (compare Section 2). As such,
488 the Etoliko record is essential in reconstructing seasonal precipitation variability
489 beyond the tree-ring-based spring/summer reconstructions and can further validate
490 model-based precipitation reconstructions in SE Europe during the latter part of the
491 LIA. In the following, we evaluate inferred precipitation variability at Etoliko for the
492 periods (i) 1740–1790 AD, i.e., between the Maunder and Dalton Solar Minima; (ii)
493 1790–1830 AD, which spans the Dalton Minimum; (iii) 1830–1930 AD, which
494 represents the latest phase of the LIA and the onset of modern warming.

495

496 **5.3.1 1740–1790 AD**

497 The interval between the Maunder and Dalton Solar Minima is characterized by
498 increased terrestrial runoff into Etoliko Lagoon. This is testified by the peaking of
499 Ti/Ca values, which is indicative of elevated clastic input into the lagoon, the strong
500 decline of $\delta^{13}\text{C}_{\text{ostracod}}$ values that points to higher input of terrestrial organic matter,
501 and increased pollen concentration in the Etoliko sediments during that time interval
502 (Figure 8). In the absence of notable changes in vegetation cover in the lagoon's
503 catchment area (compare Section 4.2), we interpret the increase of terrestrial input
504 into the lagoon to have resulted from increased precipitation and runoff in winter.

505 It has been suggested previously that high winter precipitation over Western Greece
506 during the LIA may be attributed to a combined low-pressure system over the
507 Eastern Mediterranean associated with an anticyclone in N-NE Europe (Xoplaki et
508 al., 2000, 2001). In general, winter precipitation over the Eastern Mediterranean is
509 strongly affected by the North Atlantic Oscillation (NAO; e.g., Wanner et al., 2001).
510 More specifically, the NAO comprises a large-scale meridional vacillation in air

511 masses in the North Atlantic, centred near Iceland and the Azores Islands and
512 affecting climate in Europe particularly during December–March (e.g., Wanner et al.,
513 2001). It is characterized by a positive mode causing wetter-than-average conditions
514 in northern Europe and drier conditions in the Mediterranean region, and a negative
515 mode with reversed characteristics. Model-based reconstructions indicate a
516 persistent strong negative winter NAO mode between 1740 and 1770 AD (Figure 8;
517 Luterbacher et al., 1999), which could explain the increased precipitation at Etoliko,
518 perhaps associated with a stronger orographic effect leading to elevated precipitation
519 in Western Greece (Xoplaki et al., 2000). Pairing of proxy and instrumental data
520 spanning the last century has demonstrated the sensitivity of the Etoliko aquatic
521 ecosystem to winter NAO variability even under severe human pressure on the
522 lagoon (Koutsodendris et al., 2015).

523 Tree-ring-based spring/summer precipitation reconstructions for the Balkan
524 Peninsula suggest increased precipitation for the interval 1700–1750 AD (Nicault et
525 al., 2008), with peak wet conditions during 1750–1755 AD (Touchan et al., 2005). In
526 contrast, dry conditions have been inferred for 1760–1785 AD (Nicault et al., 2008).
527 Accepting that the Etoliko data represent winter precipitation, while the tree-ring
528 reconstructions reflect spring and summer precipitation change, the coupling of both
529 datasets suggests that the interval between 1740 and 1755 AD was a period of
530 enhanced precipitation in all seasons. Instead, the interval between 1760 and 1785
531 AD was probably associated with enhanced winter precipitation only.

532

533 **5.3.2 1790–1830 AD (Dalton Minimum)**

534 The last cold episode of the LIA in Europe occurred from 1790 to 1830 AD; it has
535 been attributed to low solar forcing (i.e., Dalton Minimum *sensu stricto*) and the
536 impact of volcanic eruptions on global climate (Luterbacher et al., 2004; PAGES 2k
537 Consortium, 2013; Luterbacher and Pfister, 2015). For the Balkans, tree-ring

538 reconstructions spanning the Dalton Minimum suggest a prevalence of relatively cool
539 (Trouet, 2014; Klesse et al., 2015) and wet conditions (Nicault et al., 2008) in
540 spring/summer; in addition, historical data also document cold winters (Xoplaki et al.,
541 2001). Based on our proxy data from Etoliko, the Dalton Minimum is marked by
542 decreases in organic-rich sub-layer thickness, Ti/Ca ratios and pollen concentration,
543 and an increase of the $\delta^{13}\text{C}_{\text{ostracod}}$ values (Figure 8). Tentative evidence for an
544 associated decrease in nutrient status is given by the return to dominance by
545 *Cyclotella choctawhatcheeana* (Figure 7; e.g., Weckström and Juggins, 2005), which
546 is also in agreement with a decrease in the concentration of heterotrophic dinocysts
547 (Figure 6). These changes provide conclusive evidence for decreasing terrestrial and
548 nutrient input into the lagoon.

549 The diatom assemblages at Etoliko also show a striking change in species
550 assemblage composition between 1790 and 1830 AD. This is marked by a 20-30 %
551 increase of benthic taxa at the expense of planktonic taxa, which suggests lowering
552 of the water level at Etoliko (Figure 7). In addition, the increase in the Sr/Ca ratios
553 during the Dalton Minimum (starting at ~1790 AD; Figure 5) suggests increasing
554 salinity at Etoliko (Ariztegui et al., 2010; Morellón et al., 2016), which can be
555 attributed to higher evaporation. In concert, the Fe/Mn ratios can be explained by the
556 establishment of a stronger water-mass stratification due to increased salinity of the
557 upper water column of Etoliko Lagoon (Figure 5). Finally, support for prevalence of
558 more arid conditions is provided by the transient increase of the Mediterranean
559 sclerophylls, which typically comprise drought-resistant taxa (Figure 6).

560 In summary, the Dalton Minimum interval is characterized by reduced nutrient input,
561 lowering of the water level, increasing salinities and stronger anoxia at Etoliko, which
562 can be attributed to reduced river runoff into the lagoon. Given that tree-ring
563 spring/summer precipitation reconstructions show no evidence for drier conditions on
564 the Balkan Peninsula during the Dalton Minimum (Nicault et al., 2008), we suggest

565 that the precipitation deficit inferred for Etoliko during the 1790–1830 AD period was
566 restricted to the winter season. Considering that the positive NAO winter mode is
567 strongly associated with decreasing precipitation in winter in the Balkans (Wanner et
568 al., 2001), the transition to more positive winter NAO during the onset of the Dalton
569 Minimum (Figure 8) may have been responsible for the change of winter precipitation
570 at Etoliko. Furthermore, the decrease in winter precipitation could have been related
571 to blocking conditions caused by a southward extension of the continental
572 anticyclone over Eastern Europe that prevented the crossing of low-pressure
573 systems towards the Balkan Peninsula (e.g., Xoplaki et al., 2000, 2001).

574

575 **5.3.3 1830–1930 AD**

576 The proxy data show a complex picture regarding the precipitation variability at
577 Etoliko during 1830–1930 AD. On the one hand, the persistently high Sr/Ca ratios
578 (Figure 5) suggest a more saline aquatic environment than prior to 1830 AD. This
579 can be attributed to decreasing river runoff due to lower precipitation in winter as
580 suggested by the generally positive winter NAO mode following the Dalton Minimum
581 (Figure 8; Luterbacher et al., 1999). A drop in precipitation is confirmed by
582 instrumental data from Athens (Figure 1) extending back to 1870 AD (Katsoulis and
583 Kambetzidis, 1989). Furthermore, increased salinity is also confirmed by the biotic
584 proxies, i.e., the formation of distinct silicoflagellate sub-layers (Figure 4) and the
585 increase of dinocysts concentration in the sediments (Figure 8) particularly from 1850
586 AD onwards. These observations provide evidence for a stronger connection of
587 Etoliko Lagoon to the marine realm than during the Dalton Minimum. Considering
588 that the lagoon is formed perpendicular to the coast and connected to the sea via a
589 narrow opening (Figure 2), the sea can only intrude into Etoliko under the prevalence
590 of strong southerly winds as it has been documented by instrumental data over the
591 last decade (Gianni et al., 2011). This points to a potential strengthening of southern

592 winds over Western Greece during this period. Interestingly, the increase in marine
593 algae in the Etoliko sediments is coeval with a shift of the summer NAO to negative
594 values (Figure 8). A shift to negative summer NAO would suppress the meridional
595 circulation over the Eastern Mediterranean (Chronis et al., 2011), hence reducing the
596 influence of the northerly winds (Etesian winds) in the Balkan Peninsula. In addition,
597 the summer NAO can significantly affect atmospheric circulation and precipitation in
598 the Balkan Peninsula during summer (e.g., Chronis et al., 2011; Bladé et al., 2012)
599 and could have been responsible for reduced summer precipitation (Bladé et al.,
600 2012) and decreased cloudiness (Chronis et al., 2011). These would increase
601 evaporation and, ultimately, amplify the influence of the marine realm on the lagoon.

602 Remarkably, however, the strong variability registered in the $\delta^{18}\text{O}_{\text{ostracod}}$ values from
603 1830 AD onwards suggests transient shifts to lower salinity at Etoliko (Figure 4). High
604 amplitude variability can be also seen in the Ti counts (Figure 4) and, to a lesser
605 extent, in the $\delta^{13}\text{C}_{\text{ostracod}}$ values and dinocysts concentrations (Figure 8). These data
606 provide evidence for transiently increased inflow of freshwater into Etoliko.
607 Considering the land use changes in the Etoliko catchment area as suggested by the
608 expansion of cultivation (Figure 6), strong rainfall events might have induced soil
609 erosion and increase terrestrial input into the lagoon. Reconstructions of the winter
610 NAO show intervals with very negative values during 1850–1930 AD (Figure 8),
611 which could have been responsible for increased winter precipitation over some
612 years. This hypothesis is also in agreement with tree-ring climate reconstructions
613 from the Eastern Mediterranean region that suggest particularly high variability in the
614 atmospheric circulation and extreme wet and dry events between 1850 and 1930 AD
615 (Touchan et al., 2005).

616 Finally, another notable change in the proxy data occurs between the Dalton
617 Minimum and the recent global warming period. More specifically, the Etoliko record
618 is marked by a decrease in Ca counts (Figure 5) and the calcite sub-layers thickness

619 (Figure 8) between 1880 and 1920 AD. During the same interval, a decrease in the
620 Si/Ti ratios (Figure 5), suggests decreasing productivity at Etoliko that may have
621 influenced the calcite precipitation. Remarkably, this interval is characterized by
622 decreased summer temperature in Europe (Luterbacher et al., 2004; Xoplaki et al.,
623 2005; Lelieveld et al., 2012), which is also documented in meteorological records
624 from Athens and Kerkyra in Greece (Mariolopoulos et al., 1985; Arseni-Papadimitriou
625 and Maheras, 1991). The pervasiveness of decreased summer temperatures across
626 Europe during this interval can have influenced the diatom blooms (e.g., Winder et
627 al., 2009), hence decreasing the productivity of the lagoon and subsequently the
628 calcite precipitation.

629

630 **5.4 Longitudinal shifts of wet/dry conditions on the Balkan Peninsula**

631 A comparison of paleoclimatic data from the Western (Iberian Peninsula and NW
632 Africa) and Eastern Mediterranean (Asia Minor and Middle East) spanning the last
633 millennium has documented a see-saw pattern in precipitation during the LIA for this
634 region (e.g., Roberts et al., 2012; Corella et al., 2014). More specifically, the Western
635 Mediterranean appears to have experienced wet conditions, whereas dry conditions
636 prevailed in the Eastern Mediterranean. To date, however, the boundary between the
637 wet and dry regions during the LIA is poorly constrained. The Balkan Peninsula is
638 located in the Eastern Mediterranean region and, based on the see-saw precipitation
639 pattern, should have been influenced by dry conditions during the LIA (Roberts et al.,
640 2012). The available proxy data reveal a more complex picture (e.g., Klesse et al.,
641 2015; Cook et al., 2016; Gogou et al., 2016), however. The XRF-based Ti/Ca ratios
642 from Lake Butrint (Western Balkans; Figure 1) document wet conditions during
643 ~1600–1800 AD (Figure 8; Morellón et al., 2016). This is in agreement with the low-
644 resolution isotope records from Lakes Ohrid and Prespa (Figure 1) that also suggest
645 a prevalence of wet conditions over the last millennium in the Western Balkans (Leng
646 et al., 2013; Lacey et al., 2014). Wet conditions have been further inferred from

647 increasing terrestrial input during the last millennium in the North Aegean (core M2,
648 Figure 1; Gogou et al., 2016); however, this signal may also represent increasing
649 precipitation in the northern Balkan Peninsula where the origin of most of the rivers
650 flowing into the North Aegean is. A clear contrast is however documented in XRF-
651 based potassium data (Francke et al., 2013) from Lake Dojran (Figure 1) that show a
652 prevalence of dry conditions over the last millennium in the Eastern Balkans (Figure
653 8; Zhang et al., 2014). Based on these lines of evidence, a wet/dry pattern is evident
654 for the Balkan Peninsula during the LIA (e.g., Morellón et al., 2016). Similar to the
655 present-day precipitation distribution in the Balkans (Figure 1), the Pindos range may
656 have acted as a natural boundary, with a strong orographic effect (Xoplaki et al.,
657 2000) perhaps even amplifying the regional contrast during the LIA.

658 The Etoliko record provides detailed evidence for the precipitation variability in winter
659 during the LIA in the Balkans. More specifically, wet conditions prevailed between
660 1680 and 1790 AD, dry conditions between 1790 and 1830 AD, and generally dry
661 conditions, transiently interrupted by wet winters, between 1830 and 1930 AD.
662 Considering that Etoliko Lagoon is located on the Western Balkan Peninsula, we
663 further suggest that the wet/dry limit between the Western and Eastern
664 Mediterranean regions may have oscillated longitudinally during the LIA. More
665 specifically, the wet/dry boundary may have been located along the Pindos range or
666 even further to the East during the 1680–1790 AD interval. In contrast, during 1790–
667 1830 AD (Dalton Minimum) and until 1930 AD, the wet/dry boundary could have
668 been located further westwards in the Adriatic/Ionian Seas or even the Italian
669 Peninsula. For future research, we suggest that the spatial extent of the wet/dry
670 regions across the Mediterranean region should be further constrained via new
671 records particularly from the Eastern Balkans for which highly resolved records are
672 yet lacking.

673

674 **6. Conclusions**

675 We have evaluated a new, ~500-year-long varve record from Etoliko Lagoon
676 (Western Greece) using a multiproxy sedimentological and paleoecological
677 approach. Our results demonstrate that the aquatic ecosystem at Etoliko experienced
678 a major reorganization in the mid-18th century as reflected in a strong increase in
679 varve thickness. Following this transition, varve thickness data closely mimic solar
680 irradiance and European summer temperature trends, suggesting a sensitive
681 response of the Etoliko varve record to climate forcing. We interpret the high fidelity
682 of the Etoliko varves in recording regional climate change over the past 250 years to
683 have resulted from increased primary productivity of the lagoon beyond a critical
684 threshold, which was caused by enhanced nutrient input of both terrestrial and
685 marine origin.

686 The Etoliko record suggests considerable precipitation variability during the LIA in the
687 SW Balkan Peninsula, which can be attributed to atmospheric circulation changes
688 predominantly related to the NAO variability. Shifts between wet and dry phases at
689 Etoliko point to longitudinal shifts of the precipitation pattern in the Balkans,
690 challenging the view of prevailing dry conditions across the Peninsula during the LIA.

691

692 **7. Acknowledgments**

693 We would like to thank Jürg Luterbacher, Francesca Sangiorgi and Elena Xoplaki for
694 discussions. Technical support by Brian Brademann, Peter Dulski, Ilias Kousis and
695 Bärbel Schmincke is gratefully acknowledged. We also thank Mario Morellón and an
696 anonymous reviewer for their constructive comments. All data are available as
697 supplementary information and are archived in the Pangaea database
698 (www.pangaea.de).

699

700 **8. References**

- 701 Ariztegui, D., Anselmetti, F.S., Robbiani, J.-M., Bernasconi, S.M., Brati, E., Gilli, A.,
702 Lehmann, M.F., 2010. Natural and human-induced environmental change in southern
703 Albania for the last 300 years — Constraints from the Lake Butrint sedimentary
704 record. *Global and Planetary Change* 71, 183-192.
- 705 Arseni-Papadimitriou, A., Maheras, P., 1991. Some statistical characteristics of air
706 temperature variations at four Mediterranean stations. *Theoretical and Applied*
707 *Climatology* 43, 105-112.
- 708 Balkis, N., Balci, M., Giannakourou, A., Venetsanopoulou, A., Mudie, P., 2016.
709 Dinoflagellate resting cysts in recent marine sediments from the Gulf of Gemlik
710 (Marmara Sea, Turkey) and seasonal harmful algal blooms. *Phycologia* 55, 187-209.
- 711 Battarbee, R.W., Jones, V.J., Flower, R.J., Cameron, N.G., Bennion, H., 2001.
712 Diatoms, In: Smol, J.P., Birks, H.J.B., Last, W.M. (Eds.), *Tracking Environmental*
713 *Change Using Lake Sediments (Vol. 3): Terrestrial, Algal, and Siliceous Indicators*.
714 Kluwer Academic Publishers, Dordrecht, Netherlands, 155–202.
- 715 Bladé, I., Liebmann, B., Fortuny, van Oldenborgh, G.J., 2012. Observed and
716 simulated impacts of the summer NAP in Europe: implications for projected drying in
717 the Mediterranean region. *Climate Dynamics* 39, 709-727.
- 718 Brauer, A., Casanova, J., 2001. Chronology and depositional processes of the
719 laminated sediment record from Lac d' Annecy, French Alps. *Journal of*
720 *Paleolimnology* 25, 163-177.
- 721 Brauer, A., 2004. Annually laminated lake sediments and their palaeoclimatic
722 relevance. In: Fisher, H., Kumke, T., Lohmann, G., Flöser, G., Miller, H., von Storch,
723 H., Negendank, J.F.W. (Eds.), *The climate in historical times. Towards a synthesis of*
724 *Holocene proxy data and climate models*. Springer, Berlin, 111–129.
- 725 Brauer, A., Mangili, C., Moscariello, A., Witt, A., 2008. Palaeoclimatic implications

726 from micro-facies data of a 5900 varve time series from the Piànico interglacial
727 sediment record, southern Alps. *Palaeogeography, Palaeoclimatology,*
728 *Palaeoecology* 259, 121-135.

729 Büntgen, U., Tegel, W., Nicolussi, K., McCormick, M., Frank, D., Trouet, V., Kaplan,
730 J.O., Herzig, F., Heussner, K.U., Wanner, H., Luterbacher, J., Esper, J., 2011. 2500
731 years of European climate variability and human susceptibility. *Science* 331, 578-
732 582.

733 Delaygue, G., Bard, E., 2011. An Antarctic view of Beryllium-10 and solar activity for
734 the past millennium. *Climate Dynamics* 36, 2201-2218.

735 Chronis, T., Raitso, D.E., Kassis, D., Sarantopoulos, A., 2011. The summer North
736 Atlantic Oscillation influence on the Eastern Mediterranean. *Journal of Climate* 24,
737 5584-5596.

738 Cook, B.I., Anchukaitis, K.J., Touchan, R., Meko, D.M., Cook, E.R., 2016.
739 Spatiotemporal drought variability in the Mediterranean over the last 900 years.
740 *Journal of Geophysical Research: Atmospheres* 121, 2060-2074.

741 Corella, J.P., Brauer, A., Mangili, C., Rull, V., Vegas-Vilarrúbia, T., Morellón, M.,
742 Valero-Garcés, B.L., 2012. The 1.5-ka varved record of Lake Montcortès (southern
743 Pyrenees, NE Spain). *Quaternary Research* 78, 323-332.

744 Corella, J.P., Benito, G., Rodríguez-Lloveras, X., Brauer, A., Valero-Garcés, B.L.,
745 2014. Annually-resolved lake record of extreme hydro-meteorological events since
746 AD 1347 in NE Iberian Peninsula. *Quaternary Science Reviews* 93, 77-90.

747 Czymzik, M., Dulski, P., Plessen, B., von Grafenstein, U., Naumann, R., Brauer, A.,
748 2010. A 450-year record of spring/summer flood layers in annually laminated
749 sediments from Lake Ammersee (Southern Germany). *Water Resources Research*
750 46, W11528.

751 Czymzik, M., Brauer, A., Dulski, P., Plessen, B., Naumann, R., von Grafenstein, U.,

752 Scheffler, R., 2013. Orbital and solar forcing of shifts in Mid- to Late Holocene flood
753 intensity from varved sediments of pre-alpine Lake Ammersee (southern Germany).
754 *Quaternary Science Reviews* 61, 96-110.

755 Dulski, P., Brauer, A., Mangili, C., 2015. Combined μ -XRF and microfacies
756 techniques for lake sediment analysis. In: Croudace, I.W., Rothwell, R.G. (Eds.),
757 *Developments in Paleoenvironmental Research (Vol. 17): Micro-XRF studies of*
758 *sediment cores, Applications of a non-destructive tool for the environmental*
759 *sciences*. Springer, Dordrecht, Netherlands, 325-349.

760 Francke, A., Wagner, B., Leng, M.J., Rethemeyer, J., 2013. A Late Glacial to
761 Holocene record of environmental change from Lake Dojran (Macedonia, Greece).
762 *Climate of the Past* 9, 481-498.

763 Gianni, A., Kehayias, G., Zacharias, I., 2011. Geomorphology modification and its
764 impact to anoxic lagoons. *Ecological Engineering* 37, 1869-1877.

765 Gilabert, A., 2001. Seasonal plankton dynamics in a Mediterranean hypersaline
766 coastal lagoon: the Mar Menor. *Journal of Plankton Research* 23, 207-217.

767 Gogou, A., Triantaphyllou, M., Xoplaki, E., Izdebski, A., Parinos, C., Dimiza, M.,
768 Bouloubassi, I., Luterbacher, J., Kouli, K., Martrat, B., Toreti, A., Fleitmann, D.,
769 Rousakis, G., Kaberi, H., Athanasiou, M., Lykousis, V., 2016. Climate variability and
770 socio-environmental changes in the northern Aegean (NE Mediterranean) during the
771 last 1500 years. *Quaternary Science Reviews*, 209-228.

772 Gray, L.J., Beer, J., Geller, M., Haigh, J.D., Lockwood, M., Matthes, K., Cubasch, U.,
773 Fleitmann, D., Harrison, G., Hood, L., Luterbacher, J., Meehl, G.A., Shindell, D., van
774 Geel, B., White, W., 2010. Solar influences on climate. *Reviews of Geophysics* 48,
775 RG4001.

776 Griggs, C., DeGaetano, A., Kuniholm, P., Newton, M., 2007. A regional high-
777 frequency reconstruction of May-June precipitation in the north Aegean from oak tree

778 rings, A.D. 1089-1989. *International Journal of Climatology* 27, 1075-1089.

779 Hijmans, R.J., Cameron, S.E., Parra, J.L., Jones, P.G., Jarvis, A., 2005. Very high
780 resolution interpolated climate surfaces for global land areas. *International Journal of*
781 *Climatology* 25, 1965-1978.

782 Hughes, P.D., 2009. Little Ice Age glaciers in the Balkans: low altitude glaciation
783 enabled by cooler temperatures and local topoclimatic controls. *Earth Surface*
784 *Processes and Landforms* 35, 229-241.

785 Jones, P.D., Mann, M.E., 2004. Climate over past millennia. *Reviews of Geophysics*
786 42, RG2002.

787 Juggins, S., 2001. *The European Diatom Database. User Guide. Version 1.0.*
788 October 2001. University of Newcastle.

789 Katsoulis, B.D., Kambetzidis, H.D., 1989. Analysis of the long-term precipitation
790 series at Athens, Greece. *Climatic Change* 14, 263-290.

791 Klesse, S., Ziehmer, M., Rousakis, G., Trouet, V., Frank, D., 2015. Synoptic drivers
792 of 400 years of summer temperature and precipitation variability on Mt. Olympus,
793 Greece. *Climate Dynamics* 45, 807-824.

794 Kienel, U., Dulski, P., Ott, F., Lorenz, S., Brauer, A., 2013. Recently induced anoxia
795 leading to the preservation of seasonal laminae in two NE-German lakes. *Journal of*
796 *Paleolimnology* 50, 535-544.

797 Kotthoff, U., Koutsodendris, A., Pross, J., Schmiedl, G., Bornemann, A., Kaul, C.,
798 Marino, G., Peyron, O., Schiebel, R., 2011. Impact of Lateglacial cold events on the
799 northern Aegean region reconstructed from marine and terrestrial proxy data. *Journal*
800 *of Quaternary Science* 26, 86-96.

801 Koutsodendris, A., Brauer, A., Pälike, H., Müller, U.C., Dulski, P., Lotter, A.F., Pross,
802 J., 2011. Sub-decadal- to decadal-scale climate cyclicity during the Holsteinian

803 interglacial (MIS 11) evidenced in annually laminated sediments. *Climate of the Past*
804 7, 987-999.

805 Koutsodendris, A., Brauer, A., Zacharias, I., Putyrskaya, V., Klemt, E., Sangiorgi, F.,
806 Pross, J., 2015. Ecosystem response to human- and climate-induced environmental
807 stress on an anoxic coastal lagoon (Etoliko, Greece) since 1930 AD. *Journal of*
808 *Paleolimnology* 53, 255-270.

809 Lacey, J.H., Francke, A., Leng, M.J., Vane, C.H., Wagner, B., 2014. A high-resolution
810 Late Glacial to Holocene record of environmental change in the Mediterranean from
811 Lake Ohrid (Macedonia/Albania). *International Journal of Earth Sciences* 104, 1623-
812 1638.

813 Leng, M., Wagner, B., Boehm, A., Panagiotopoulos, K., Vane, C.H., Snelling, A.,
814 Haidon, C., Woodley, E., Vogel, H., Zanchetta, G., Banerji, I., 2013. Understanding
815 past climatic and hydrological variability in the Mediterranean from Lake Prespa
816 sediment isotope and geochemical record over the Last Glacial cycle. *Quaternary*
817 *Science Reviews* 66, 123-136.

818 Levanic, T., Poljanek, S., Toromani, E., 2015. Early summer temperatures
819 reconstructed from black pine (*Pinus nigra* Arnold) tree-ring widths from Albania. *The*
820 *Holocene* 25, 469-481.

821 Ljungqvist, F.C., Krusic, P.J., Brattström, G., Sundqvist, H.S., 2012. Northern
822 Hemisphere temperature patterns in the last 12 centuries. *Climate of the Past* 8, 227-
823 249.

824 Ljungqvist, F.C., Krusic, P.J., Sundqvist, H.S., Zorita, E., Brattström, G., Frank, D.,
825 2016. Northern Hemisphere hydroclimate variability over the past twelve centuries.
826 *Nature* 532, 94-98.

827 Lelieveld, J., Hadjinicolaou, P., Kostopoulou, E., Chenoweth, J., El Maayar, M.,
828 Giannakopoulos, C., Hannides, C., Lange, M.A., Tanarhte, M., Tyrlis, E., Xoplaki, E.,

829 2012. Climate change and impacts in the Eastern Mediterranean and the Middle
830 East. *Climatic Change* 114, 667-687.

831 Lionello, P., Abrantes, F., Congedi, L., Dulac, F., Gacic, M., Gomis, D., Goodess, C.,
832 Hoff, H., Kutiel, H., Luterbacher, J., Planton, S., Reale, M., Schröder, K., Struglia,
833 M.V., 2012. Introduction: Mediterranean Climate—Background Information. In:
834 Lionello, P. (Ed.), *The climate of the Mediterranean region: From the past to the*
835 *future*. Elsevier, xxxv-xxc.

836 Luterbacher, J., Schmutz, C., Gyalistras, D., Xoplaki, E., Wanner, H., 1999.
837 Reconstruction of monthly NAO and EU indices back to AD 1675. *Geophysical*
838 *Research Letters* 26, 2745-2748.

839 Luterbacher, J., Dietrich, D., Xoplaki, E., Grosjean, M., Wanner, H., 2004. European
840 seasonal and annual temperature variability, trends, and extremes since 1500.
841 *Science* 303, 1499-1503.

842 Luterbacher, J., Koenig, S.J., Franke, J., van der Schrier, G., Zorita, E., Moberg, A.,
843 Jacobeit, J., Della-Marta, P.M., Küttel, M., Xoplaki, E., Wheeler, D., Rutishauser, T.,
844 Stössel, M., Wanner, H., Brazdil, R., Dobrovolny, P., Camuffo, D., Bertolin, C., van
845 Engelen, A., Gonzaley-Rouco, F.J., Wilson, R., Pfister, C., Limanowka, D., Nordli, O.,
846 Leijonhufvud, L., Söderber, J., Allan, R., Barriendos, M., Glaser, R., Riemann, D.,
847 Hao, Z., Zerefos, C.S., 2010. Circulation dynamics and its influence on European and
848 Mediterranean January–April climate over the past half millennium: results and
849 insights from instrumental data, documentary evidence and coupled climate models.
850 *Climatic Change* 101, 201-234.

851 Luterbacher, J., García-Herrera, R., Akcer-On, S., Allan, R., Alvarez-Castro, M.-C.,
852 Benito, G., Booth, J., Büntgen, U., Cagatay, N., Colombaroli, D., Davis, B., Esper, J.,
853 Felis, T., Fleitmann, D., Frank, D., Gallego, D., Garcia-Bustamante, E., Glaser, R.,
854 Gonzalez-Rouco, F.J., Goosse, H., Kiefer, T., Macklin, M.G., Manning, S.W.,

855 Montagna, P., Newman, L., Power, M.J., Rath, V., Ribera, P., Riemann, D., Roberts,
856 N., Sicre, M.-A., Silenzi, S., Tinner, W., Tzedakis, P.C., Valero-Garcés, B., van der
857 Schrier, G., Vannièrè, B., Vogt, S., Wanner, H., Werner, J.P., Willett, G., Williams,
858 M.H., Xoplaki, E., Zerefos, C.S., Zorita, E., 2012. A Review of 2000 Years of
859 Paleoclimatic Evidence in the Mediterranean. In: Lionello, P. (Ed.), *The climate of the*
860 *Mediterranean region: From the past to the future*. Elsevier, 87-185.

861 Luterbacher, J., Pfister, C., 2015. The year without a summer. *Nature Geoscience* 8,
862 246-248.

863 Mann, M. E., Bradley, R.S., Hughes, M.K., 1998. Global scale temperature patterns
864 and climate forcing over the past six centuries. *Nature* 392, 779–787.

865 Mann, M.E., Zhang, Z., Rutherford, S., Bradley, R.S., Hughes, M.K., Shindell, D.,
866 Ammann, C., Faluvegi, G., Ni, F., 2009. Global signatures and dynamical origins of
867 the Little Ice Age and Medieval Climate Anomaly. *Science* 326, 1256-1260.

868 Mariolopoulos, G.E., Repapis, C.C., Zampaka, J.C., 1985. 'Air temperature
869 observations', *Compilation of the existing meteorological observations of the town of*
870 *Kerkyra (1809-1984) Volume 1*. Research Centre for Atmospheric Physics and
871 *Climatology, Academy of Athens, Athens (in Greek)*.

872 Martín-Puertas, C., Valero-Garcés, B.L., Mata, M.P., Moreno, A., Giralt, S., Martínez-
873 Ruiz, F., Jiménez-Espejo, F., 2011. Geochemical processes in a Mediterranean
874 Lake: a high-resolution study of the last 4,000 years in Zoñar Lake, southern Spain.
875 *Journal of Paleolimnology* 46, 405-421.

876 Martín-Puertas, C., Matthes, K., Brauer, A., Muscheler, R., Hansen, F., Petrick, C.,
877 Aldahan, A., Possnert, G., van Geel, B., 2012. Regional atmospheric circulation shifts
878 induced by a grand solar minimum. *Nature Geoscience* 5, 397-401.

879 Matthews, J.A., Briffa, K.R., 2005. The 'Little Ice Age': Re-evaluation of an evolving
880 concept. *Geografiska Annaler* 87A, 17-36.

881 Mayewski, P.A., Rohling, E.E., Curt Stager, J., Karlén, W., Maasch, K.A., David
882 Meeker, L., Meyerson, E.A., Gasse, F., van Kreveld, S., Holmgren, K., Lee-Thorp, J.,
883 Rosqvist, G., Rack, F., Staubwasser, M., Schneider, R.R., Steig, E.J., 2004.
884 Holocene climate variability. *Quaternary Research* 62, 243-255.

885 Miho, A., Witkowski, A., 2005. Diatom (Bacillariophyta) flora of Albanian coastal
886 wetlands taxonomy and ecology: A review. *Proceedings of the California Academy of*
887 *Sciences*, 56, 129-145.

888 Morellón, M., Anselmetti, F.S., Ariztegui, D., Brushulli, B., Sinopoli, G., Wagner, B.,
889 Sadori, L., Gilli, A., Pambuku, A., 2016. Human-climate interactions in the central
890 Mediterranean region during the last millennia: The laminated record of Lake Butrint
891 (Albania). *Quaternary Science Reviews* 136, 134-152.

892 Mudie, P.J., Marret, F., Rochon, A., Aksu, A.E., 2010. Non-pollen palynomorphs in
893 the Black Sea corridor. *Vegetation History and Archaeobotany* 19, 531-544.

894 Mudie, P.J., Leroy, S.A.G., Marret, F., Gerasimenko, N., Kholeif, S.E.A., Sapelko, T.,
895 Filipova-Marinova, M., 2011. Non-pollen palynomorphs: Indicators of salinity and
896 environmental change in the Caspian–Black Sea–Mediterranean corridor. In
897 Buynevich, I., Yanko-Hombach, V., Gilbert, A.S., and Martin, R.E. (Eds.), *Geology*
898 *and Geoarchaeology of the Black Sea Region: Beyond the Flood Hypothesis*.
899 *Geological Society of America Special Paper* 473, 89-115.

900 Neugebauer, I., Brauer, A., Schwab, M.J., Dulski, P., Frank, U., Hadzhiivanova, E.,
901 Kitagawa, H., Litt, T., Schiebel, V., Taha, N., Waldmann, N.D., 2015. Evidences for
902 centennial dry periods at 3300 and 2800 cal. yr BP from micro-facies analyses of the
903 Dead Sea sediments. *The Holocene* 25, 1358-1371.

904 Nicault, A., Alleaume, S., Brewer, S., Carrer, M., Nola, P., Guiot, J., 2008.
905 Mediterranean drought fluctuation during the last 500 years based on tree-ring data.
906 *Climate Dynamics* 31, 227-245.

907 Nowaczyk, N.R, 2001. Logging of magnetic susceptibility. *Tracking Environmental*
908 *Change Using Lake Sediments Volume 1: Basin Analysis, Coring, and Chronological*
909 *Techniques*. Last, W.M., Smol, J.P. (Eds.), Springer, Netherlands, 155-170.

910 Ojala, A.E.K., Francus, P., Zolitschka, B., Besonen, M., Lamoureux, S.F., 2012.
911 *Characteristics of sedimentary varve chronologies – A review. Quaternary Science*
912 *Reviews* 43, 45-60.

913 PAGES 2k Consortium, 2013. Continental-scale temperature variability during the
914 past two millennia. *Nature Geoscience* 6, 339-346.

915 Panagiotopoulos, K., 2013. Late Quaternary ecosystem and climate interactions in
916 SW Balkans inferred from Lake Prespa sediments. PhD thesis, University of
917 Cologne, 194 p.

918 Reed, J.M., Stevenson, A.C., Juggins, S., 2001. A multi-proxy record of Holocene
919 climatic change in southwestern Spain: the Laguna de Medina, Cadiz. *The Holocene*
920 11, 707-719.

921 Reed, J.M., Mesquita-Joanes, F., Griffiths, H.I., 2012. Multi-indicator conductivity
922 transfer functions for Quaternary palaeoclimate reconstruction. *Journal of*
923 *Paleolimnology* 47, 251-275.

924 Resende, P., Azeiteiro, U.M., Goncalves, F., Pereira, M.J., 2007. Distribution and
925 ecological preferences of diatoms and dinoflagellates in the west Iberian coastal
926 zone (North Portugal). *Acta Oecologica* 32, 224–235.

927 Roberts, N., Moreno, A., Valero-Garcés, B.L., Corella, J.P., Jones, M., Allcock, S.,
928 Woodbridge, J., Morellón, M., Luterbacher, J., Xoplaki, E., Türkeş, M., 2012.
929 Palaeolimnological evidence for an east–west climate see-saw in the Mediterranean
930 since AD 900. *Global and Planetary Change* 84-85, 23-34.

931 Sarno, D., Zingone, A., Saggiomo, V., Carrada, G., 1993. Phytoplankton biomass
932 and species composition in a Mediterranean coastal lagoon. *Hydrobiologia* 271, 27-

933 40.

934 Schwalb, A., 2003. Lacustrine ostracodes as stable isotope recorders of late-glacial
935 and Holocene environmental dynamics and climate. *Journal of Paleolimnology* 29,
936 267-351.

937 Swierczynski, T., Brauer, A., Lauterbach, S., Martin-Puertas, C., Dulski, P., von
938 Grafenstein, U., Rohr, C., 2012. A 1600 yr seasonally resolved record of decadal-
939 scale flood variability from the Austrian Pre-Alps. *Geology* 40, 1047-1050.

940 Touchan, R., Xoplaki, E., Funkhouser, G., Luterbacher, J., Hughes, M.K., Erkan, N.,
941 Akkemik, Ü., Stephan, J., 2005. Reconstructions fo spring/summer precipitation for
942 the Eastern Mediterranean from tree-ring widths and its connection to large-scale
943 atmospheric circulation. *Climate Dynamics* 25, 75-98.

944 Triantaphyllou, M.V., Gogou, A., Bouloubassi, I., Dimiza, M., Kouli, K., Rousakis, G.,
945 Kotthoff, U., Emeis, K.C., Papanikolaou, M., Athanasiou, M., Parinos, C., Ioakim, C.,
946 Lykousis, V., 2014. Evidence for a warm and humid Mid-Holocene episode in the
947 Aegean and northern Levantine Seas (Greece, NE Mediterranean). *Regional
948 Environmental Change* 14, 1697-1712.

949 Trouet, V., 2014. A tree-ring based late summer temperature reconstruction (AD
950 1675–1980) for the Northeastern Mediterranean. *Radiocarbon* 56, S69-S78.

951 Vött, A., Schriever, A., Handl, M., Brückner, H., 2007. Holocene palaeogeographies
952 of the Eastern Acheloos river delta and the lagoon of Etoliko (NW Greece). *Journal of
953 Coastal Research* 234, 1042-1066.

954 Wanner, H., Brönnimann, S., Casty, C., Gyalistras, D., Luterbacher, J., Schmutz, C.,
955 Stephenson, D.B., Xoplaki, E., 2001. North Atlantic Oscillation - Concepts and
956 studies. *Surveys in Geophysics* 22, 321-382.

957 Weckström, K., Juggins, S., 2005. Coastal diatom-environment relationships from the
958 Gulf of Finland, Baltic Sea. *Journal of Phycology* 42, 21-35.

959 Winder, M., Reuter, J.E., Schladow, S.G., 2009. Lake warming favours small-sized
960 planktonic diatom species. *Proceedings of the Royal Society B* 276, 427-435.

961 Witkowski, A., Lange-Bertalot, H., Metzeltin, D., 2000. Annotated diatom
962 micrographs: Diatom flora of marine coasts I. *Iconographia Diatomologica* 7, Lange-
963 Bertalot, H (Ed.), ARG Gantner Verlag KG, Königstein, Germany, 925 pp.

964 Woollings, T., Lockwood, M., Masato, G., Bell, C., Gray, L., 2010. Enhanced
965 signature of solar variability in Eurasian winter climate. *Geophysical Research Letters*
966 37, L20805.

967 Xoplaki, E., Luterbacher, J., Burkard, R., Patrikas, I., Maheras, P., 2000. Connection
968 between the large-scale 500 hPa geopotential height fields and precipitation over
969 Greece during wintertime. *Climate Research* 14, 129-146.

970 Xoplaki, E., Maheras, P., Luterbacher, J., 2001. Variability of climate in meridional
971 Balkans during the periods 1675–1715 and 1780–1830 and its impact on human life.
972 *Climatic Change* 48, 581-615.

973 Xoplaki, E., Luterbacher, J., Paeth, H., Dietrich, D., Steiner, N., Grosjean, M.,
974 Wanner, H., 2005. European spring and autumn temperature variability and change
975 of extremes over the last half millennium. *Geophysical Research Letters* 32, L15713.

976 Xoplaki, E., Fleitmann, D., Luterbacher, J., Wagner, S., Haldon, J.F., Zorita, E.,
977 Telelis, I., Toreti, A., Izdebski, A., 2016. The Medieval Climate Anomaly and
978 Byzantium: A review of the evidence on climatic fluctuations, economic performance
979 and societal change. *Quaternary Science Reviews* 229-252.

980 Zhang, X., Reed, J., Wagner, B., Francke, A., Levkov, Z., 2014. Lateglacial and
981 Holocene climate and environmental change in the northeastern Mediterranean
982 region: diatom evidence from Lake Dojran (Republic of Macedonia/Greece).
983 *Quaternary Science Reviews* 103, 51-66.

984 Zolitschka, B., Francus, P., Ojala, A.E.K., Schimmelmann, A., 2015. Varves in lake

985 sediments – a review. *Quaternary Science Reviews* 117, 1-41.

986

987 **Figure legends**

988

989 **Figure 1:** Relief map of the southern Balkan Peninsula with temperature (right) and
990 precipitation (left) data for the period 1950–2000 (Hijmans et al., 2005; modified from
991 Panagiotopoulos, 2013). Etoliko Lagoon and other key sites discussed in the text are
992 indicated. (2-COLUMN FITTING IMAGE)

993 **Figure 2:** Map of Etoliko Lagoon and surrounding area. The coring location is
994 indicated with a star. (SINGLE COLUMN FITTING IMAGE)

995 **Figure 3:** Photographs and magnetic susceptibility data of the cores from Etoliko
996 Lagoon used in this study. (SINGLE COLUMN FITTING IMAGE)

997 **Figure 4:** Total varve and selected varve sub-layer thicknesses, and ostracod-based
998 oxygen and carbon isotope data from Etoliko Lagoon between 1450 and 1930 AD.
999 Black horizontal line marks 1740 AD. DM: Dalton Minimum; MM: Maunder Minimum.
1000 Note reversed axis for $\delta^{13}\text{C}_{\text{ostracod}}$. (1.5- OR 2-COLUMN FITTING IMAGE)

1001 **Figure 5:** μ -XRF scanning data for Ca, Ti, and Fe/Mn, Si/Ti, Sr/Ca, Ti/Ca elemental
1002 ratios for the Etoliko sediments between 1450 and 1930 AD. Note logarithmic axes
1003 for Fe/Mn and Sr/Ca. No data are shown for intervals of poor varve preservation.
1004 Black horizontal line marks 1740 AD. DM: Dalton Minimum; MM: Maunder Minimum.
1005 (1.5- OR 2-COLUMN FITTING IMAGE)

1006 **Figure 6:** Pollen and dinoflagellate cyst assemblages from Etoliko Lagoon between
1007 1450 and 1930 AD. Gray bars in pollen groups and phototrophic/autotrophic plots
1008 represent pollen grain and dinocyst concentrations in the sediment, respectively.
1009 Black horizontal line marks 1740 AD. DM: Dalton Minimum; MM: Maunder Minimum.
1010 (2-COLUMN FITTING IMAGE)

1011 **Figure 7:** Relative abundance of selected diatom taxa at Etoliko Lagoon between
1012 1450 and 2010 AD. Black horizontal line marks 1740 AD. DM: Dalton Minimum; MM:
1013 Maunder Minimum. (2-COLUMN FITTING IMAGE)

1014 **Figure 8:** Selected proxy data from Etoliko Lagoon plotted against ^{10}Be -based total
1015 solar irradiance variability measured in Antarctic ice cores (Delaygue and Bard,
1016 2011), mean summer European temperature reconstructions (June-July-August
1017 [JJA]; Luterbacher et al., 2004; Xoplaki et al., 2005), North Atlantic Oscillation index
1018 for winter (DJF: December-January-February) and summer (JJA: June-July-August)
1019 (Luterbacher et al. 1999), and XRF scanning data from Lakes Butrint (Ti/Ca ratios;
1020 Morellón et al., 2016) and Dojran (K; Francke et al., 2013). Note reversed axis for
1021 $\delta^{13}\text{C}_{\text{ostracod}}$ and benthic diatom percentages. Black horizontal line marks 1740 AD.
1022 DM: Dalton Minimum; MM: Maunder Minimum. (2-COLUMN FITTING IMAGE)

Figure 1
[Click here to download high resolution image](#)

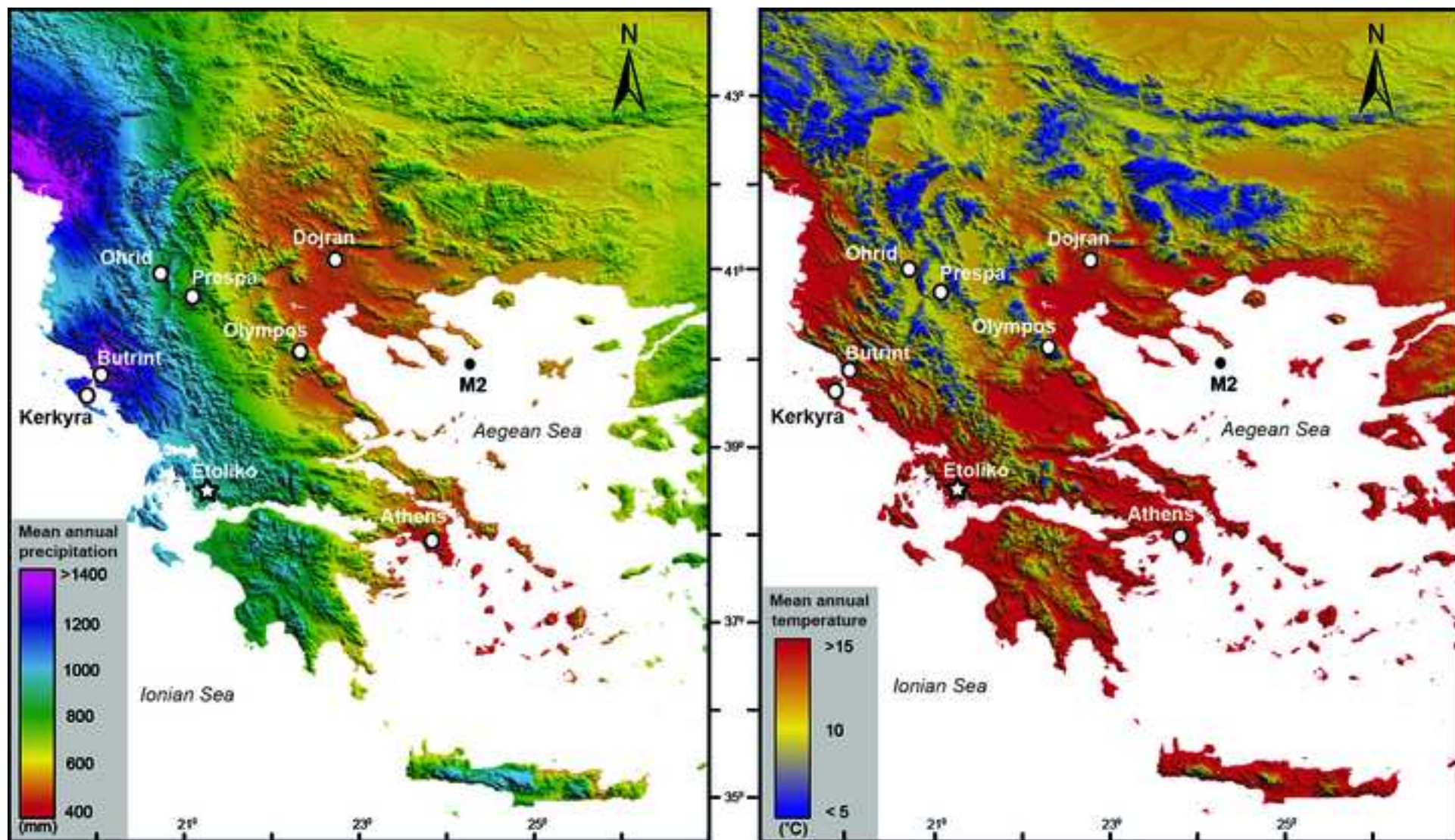


Figure 2
Click here to download high resolution image



Figure 3
[Click here to download high resolution image](#)

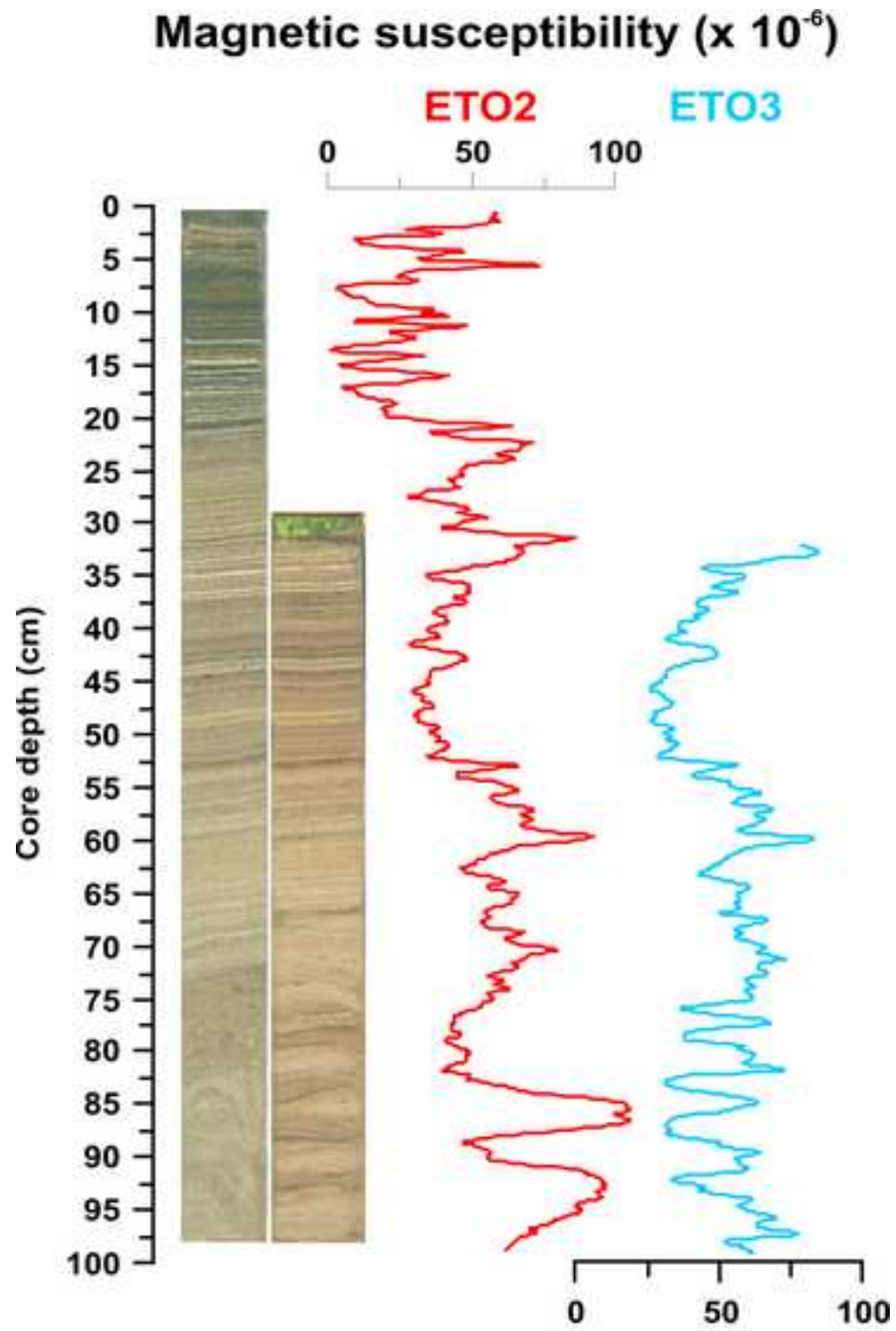


Figure 4
[Click here to download high resolution image](#)

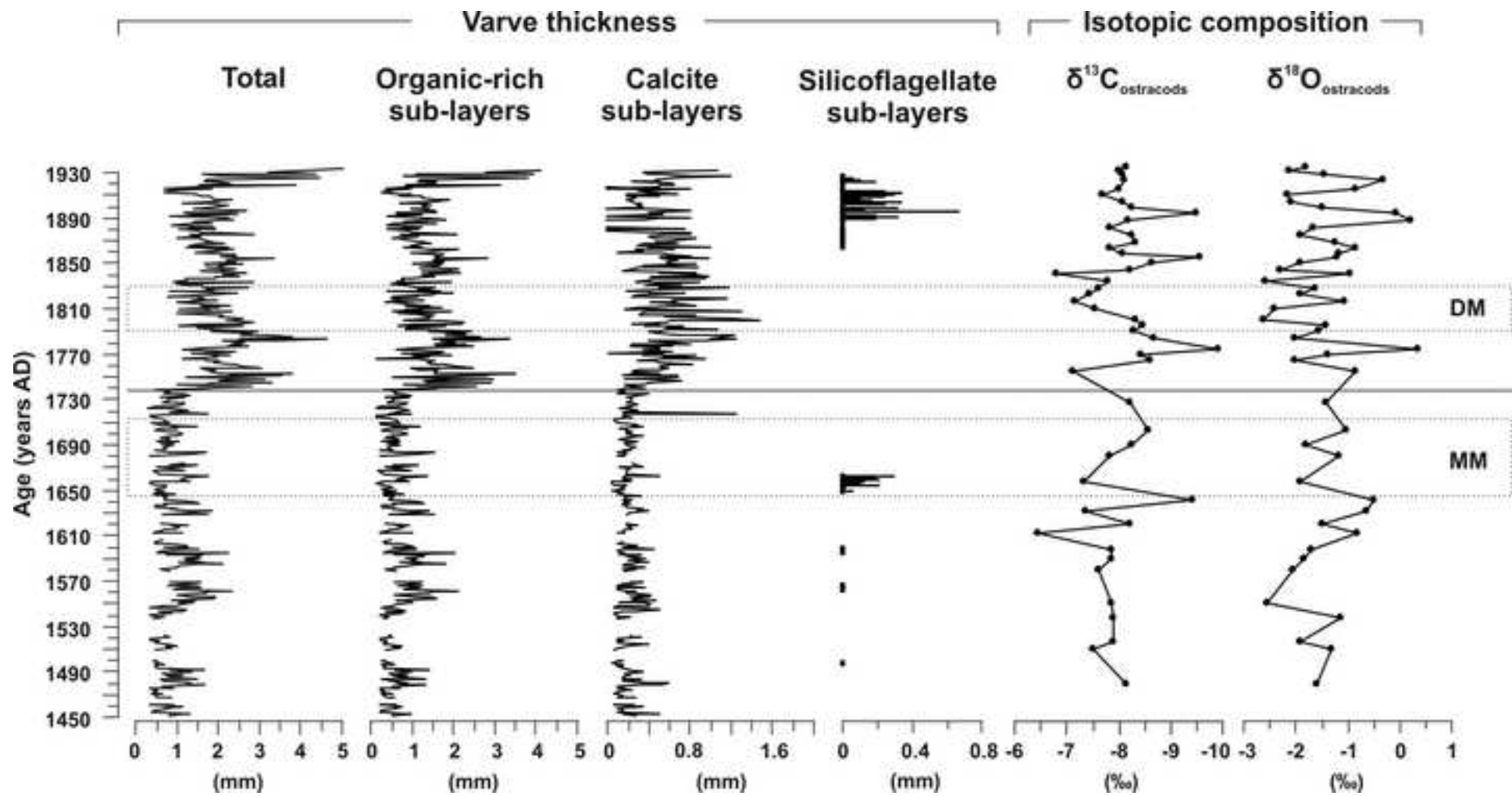


Figure 5
[Click here to download high resolution image](#)

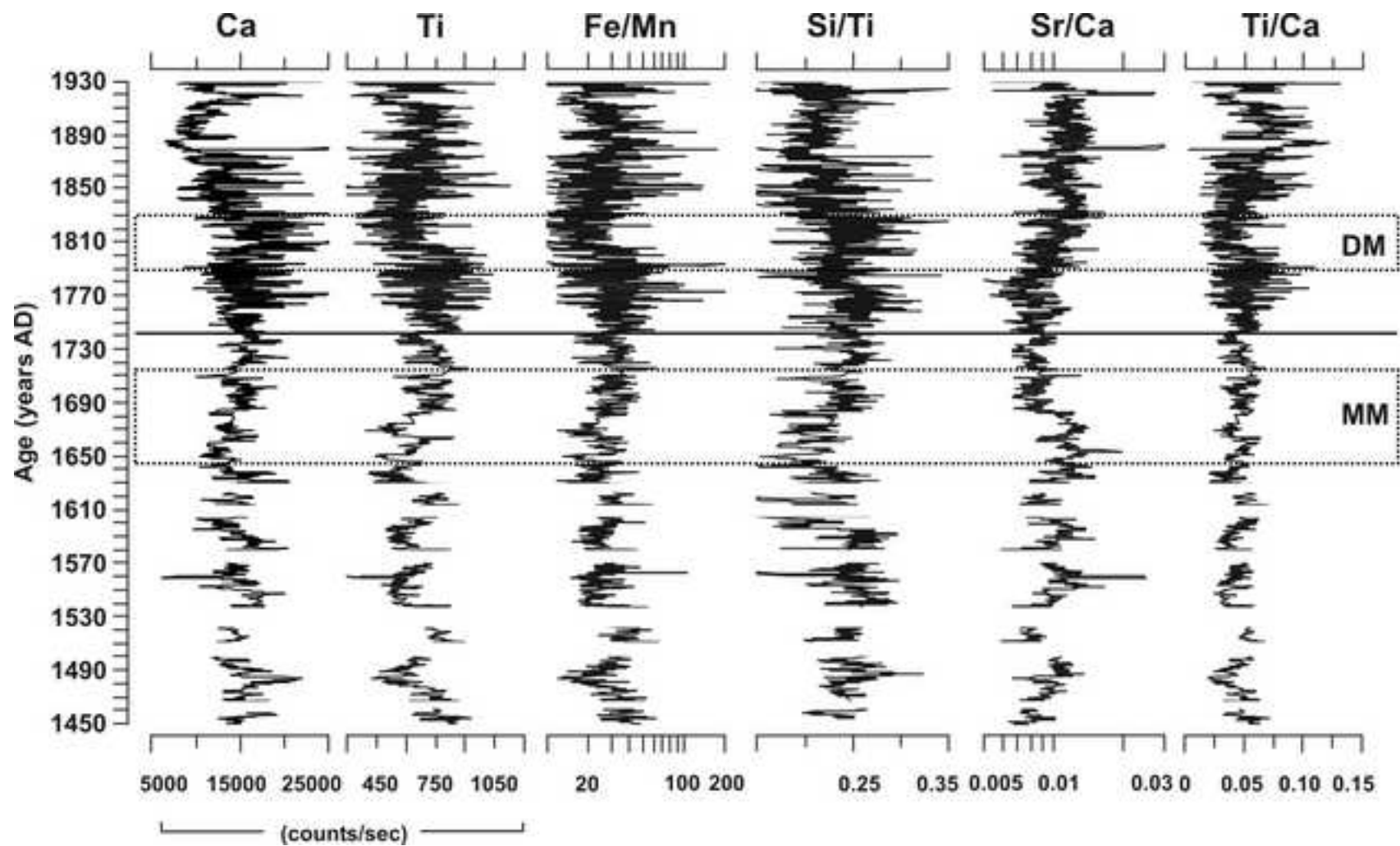


Figure 7
[Click here to download high resolution image](#)

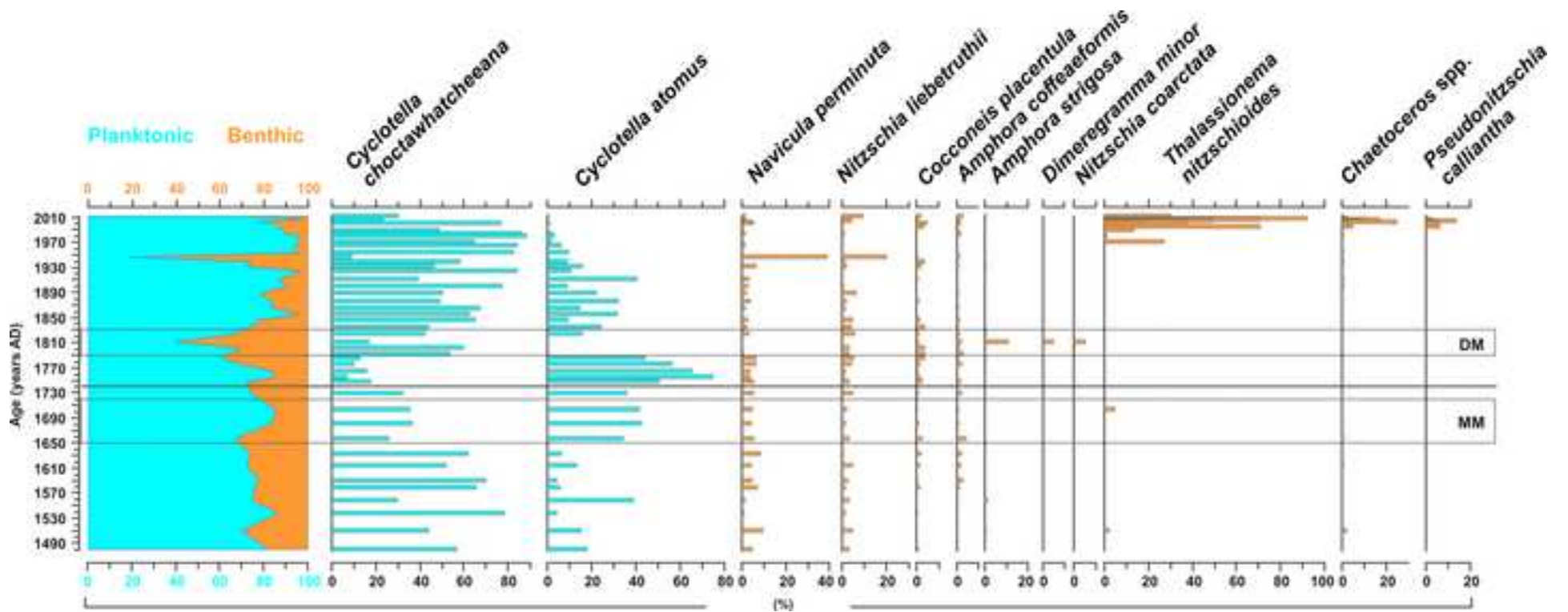


Figure 8
[Click here to download high resolution image](#)

